Analysis of long range correlations due to coherent light scattering from *in-vitro* cell arrays using angle-resolved low coherence interferometry

John W. Pyhtila
Hongwei Ma
Andrew J. Simnick
Ashutosh Chilkoti
Adam Wax
Duke University
Department of Biomedical Engineering
Fitzpatrick Center for Photonics
Durham, North Carolina 27708
E-mail: a.wax@duke.edu

Abstract. Angle-resolved low coherence interferometry (a/LCI) enables depth-resolved measurements of scattered light that can be used to recover subsurface structural information, such as the size of cell nuclei. Measurements of nuclear morphology, however, can be complicated by coherent scattering between adjacent cell nuclei. Previous studies have eliminated this component by applying a window filter to Fourier transformed angular data, based on the justification that the coherent scattering must necessarily occur over length scales greater than the cell size. To fully study this effect, results of experiments designed to test the validity of this approach are now presented. The a/LCI technique is used to examine light scattered by regular cell arrays, created using stamped adhesive micropatterned substrates. By varying the array spacing, it is demonstrated that cell-to-cell correlations have a predictable effect on light scattering distributions. These results are compared to image analysis of fluorescence micrographs of the cell array samples. The a/LCI results show that the impact of coherent scattering on nuclear morphology measurements can be eliminated through data filtering. © *2006 Society of Photo-Optical Instrumentation Engineers.* [DOI: 10.1117/1.2209561]

Keywords: low coherence interferometry; scattering measurements; cell arrays.

1 Introduction

Elastically scattered light can be used to obtain structural information in biological applications. It has been used previously to study cellular morphology[1–4] as well as to diagnose dysplasia, a precancerous tissue state.[5–8] Angle-resolved low coherence interferometry (a/LCI) has been developed as a means to obtain structural information from subsurface sites by examining the angular distribution of scattered light.[9–11] The a/LCI technique combines the ability of low coherence interferometry to detect singly scattered light from subsurface sites with the capability of light scattering methods to obtain structural information with subwavelength precision and accuracy.[2,6] a/LCI has been successfully applied to measuring cellular morphology *in vitro*[2] and in tissues,[10] as well as diagnosing intraepithelial neoplasia[6] and assessing the efficacy of chemopreventive agents[12] in an animal model of carcinogenesis. The latter study was significant because it used a/LCI to prospectively grade tissue samples without tissue processing, demonstrating the potential of the technique as a clinical diagnostic.

The a/LCI technique was first used to probe nuclear morphology in a study of *in-vitro* HT29 epithelial cells, a line of human tumor cells.[2] This study outlined an analysis for comparing scattering by nonspherical cell nuclei to the predictions of Mie theory, and demonstrated subwavelength precision and accuracy in determining nuclear size. In addition, the a/LCI study of HT29 cells was the first to identify that long range correlations between adjacent cells could be observed using the technique. When a/LCI is used to make nuclear structure measurements, the long range correlations are suppressed by applying a low pass filter. This step is justified by the fact that long range correlations cause high frequency oscillations in the angular data.

In this work, the effect of coherent scattering by adjacent cells on a/LCI measurements of nuclear morphology is examined. We have applied a/LCI to investigate light scattered by cell arrays, in which the distance between adjacent cells is systematically varied, providing a unique opportunity to examine the effects of coherent scattering by adjacent cell nuclei. The results are compared to correlation data obtained by image analysis to show that a/LCI can observe long range cell-to-cell correlations. It is further demonstrated that the effects of these correlations can be filtered out such that they do not impact the structural measurements made using the a/LCI technique. While previous a/LCI studies with animal

Address all correspondence to Adam Wax, Biomedical Engineering, Duke Univ., Box 90281, Durham, NC 27708 United States of America; Tel: 919 660 2508; Fax: 919 660-2525; E-mail: a.wax@duke.edu
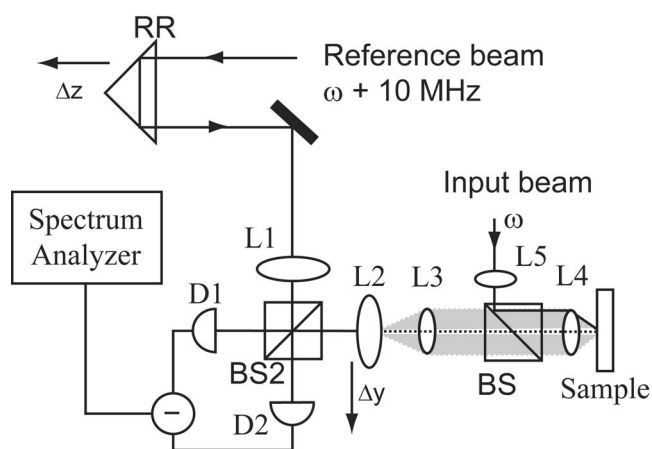
Fig. 1 Schematic of new a/LCI system. L1 through L5 are lenses, BS1 and BS2 are beamsplitters, D1 and D2 are balanced detectors, and RR is the retroreflector. The shaded area shows scattered light.

tissues[6,12] have shown that useful diagnostic information is obtained, regardless of the basis of the filtering step, future studies will benefit by establishing the relationship between high frequency oscillations and long range correlations.

2 Materials and Methods

2.1 Experimental Scheme

The experiments use a heterodyne a/LCI interferometer (Fig. 1), described previously.[10] Briefly, depth resolution is achieved by using the optical output of a Ti:sapphire laser ($\lambda_o = 870$ nm, *coherence* length$= 30 \ \mu$m) in a modified Mach-Zehnder interferometer geometry. This system acquires a single depth scan at one scattering angle in approximately seven seconds, a fraction of the time needed with previous Michelson-based systems. The scheme achieves fast acquisition rates through the use of acousto-optic modulators to offset the signal and reference fields in frequency, resulting in a heterodyne beat signal of 10 MHz when the two fields are mixed at beamsplitter BS2, a significantly higher heterodyne frequency than that of previous a/LCI systems.

The heterodyne a/LCI system employs several imaging lenses to detect the angular distribution of scattered light. The imaging system is aligned using a standard scattering sample where misalignment is evident by uneven or lack of scattered light detection. Lenses L3 and L4 ($f_3 = 10$ cm, $f_4 = 3.5$ cm) comprise a $4f$ imaging system that collects the scattered light and images the phase and amplitude of the scattered field onto the plane of lens L2. The unequal focal lengths of L3 and L4 cause a magnification of the scattered field by 10/3.5, which also has the effect of scaling down the angular distribution by 0.35. The numerical aperture of this $4f$ system sets the range of detectable angles to 0.65 rad. The angular range and sampling of the angular distribution govern the resolution and range of the detected spatial correlations. The impact of these parameters on probing long range correlations in the cell array samples is discussed later.

Both the reference field and the scattered field pass through imaging lenses before they are combined at BS2. Lens L2 ($f_2 = 10$ cm) is mechanically translated to serially scan the detected scattering angle. Lens L1 ($f_1 = 10$ cm) is included to alter the wavefront of the reference field to compensate for the effects of L2. The role of lens L5 ($f_5 = 10$ cm) is to alter the wavefront of the input beam to the sample, such that L4 recollimates it rather than focusing it. The result is a collimated beam reaching the sample with a 0.35 mm diameter and a corresponding diffraction angle of 1.8 mrad. The narrow angular distribution of the input beam is essential, since using light traveling at many angles will smear the angular scattering patterns. In addition to this role, the lateral displacement of L5 relative to L4 allows the full angular aperture of the lenses to be used to detect angular scattering distributions. The input beam strikes the sample obliquely, avoiding obscuring the scattered light by specular reflection. Note, however, that the exact backscattering direction is antiparallel to the input beam, regardless of the orientation of the sample surface.

2.2 Image Analysis

To assess the accuracy of the a/LCI nuclear morphology measurements, ImageJ software [National Institutes of Health (NIH), Bethesda, MD] was used to execute quantitative image analysis (QIA) of stained cell samples. Cell nuclei were stained with Hoechst 33342 (Invitrogen, Carlsbad, CA) and visualized using fluorescence microscopy (Axiovert 200, Zeiss, Oberkochen, Germany). The major and minor axis of each cell nuclei was measured manually and the geometric mean determined to assess the nuclear diameter. QIA of a large number of cell nuclei was used to determine the average nuclear size for the cell samples.

To assess the accuracy of the long range correlation measurements, QIA was executed to obtain autocorrelation data of fluorescence micrographs using ImageJ software and Mathematica (Wolfram Research, Champaign, IL). The average nearest-neighbor distance was found by computing the autocorrelation function $\Gamma(r)$ for a horizontal image segment:

$$\Gamma(r) = \int I(x)I(x+r)dx, \qquad (1)$$

where $I(x)$ is the intensity of the image at point x and r is the correlation distance. Both the direction specified by the correlation distance r and the direction defined by the detected scattering angle are chosen to lie along the direction of the sites in the cell array. The nearest-neighbor spacing was taken to be the first peak observed at a nonzero correlation distance.

2.3 Cell Culture

NIH/3T3 fibroblasts, which have a nuclear diameter on the order of 10 μm and a spindly irregular cell structure roughly three times the nuclear diameter, were grown in DMEM with 10% calf serum (Invitrogen), at 37°C in 5% CO_2. Culture media was supplemented with 100-units/mL penicillin and 100-μg/mL streptomycin. Cells near confluence were detached from the tissue culture flask using 0.25% trypsin-EDTA (Invitrogen) and seeded onto micropatterned or unpatterned control substrates at a density of 120,000 cells/cm^2. The culture medium was changed 3-h postseeding to remove

floating, dead cells. The a/LCI data, phase contrast, and fluorescence microscopy images were acquired 24 h after initial seeding.

2.4 Cell Arrays

Cell arrays were fabricated using the procedures outlined by Hyun et al.[13] and Ma et al.[14] A comb polymer was micropatterned using an oxidized poly(dimethyl siloxane) (PDMS) stamp presenting micrometer-sized negative features. The stamp was then spin-coated with a 100-mg/mL solution of the comb polymer in a 20:80 (v/v) H_2O/methanol mixture, and brought into conformal contact with the clean, unmodified glass surface. The comb polymer pattern was cured in an oven under vacuum at $60\,^\circ$C overnight. The resulting surface was then incubated with a 50-μg/mL fibronectin solution in phosphate buffered saline (PBS) for 1 h at room temperature and then rinsed with deionized water.

2.5 Cell Array Design for Angle-Resolved Low Coherence Interferometry

In previous cell array studies, NIH/3T3 cells were cultured on a square micropatterned array with 10-μm-diameter adhesion sites and 40-μm spacing between cells.[13,14] This optimal arrangement, resulting in isolated cells on individual adhesion sites, has a center-to-center distance between sites of 50 μm, and thus is termed a 50-μm period array. The 50-μm period array, although optimal for isolating individual 3T3 cells, is not well suited for examining long range correlations using a/LCI. In past a/LCI experiments, 30 to 40 points were used to sample the angular distribution over a 0.3- to 0.4-rad range.[2,10,11] This range was chosen to examine nuclear features in the 5- to 15-μm range and thus was only able to detect spatial correlations as large as 40 μm. Thus, the data acquisition and cell array parameters needed to be altered to observe long range correlations with a/LCI.

Three steps were taken to enable a/LCI detection of long range correlations: 1. the sampling of the a/LCI probe was increased to 60 to 70 points; 2. the angular range was decreased to 0.32 rad, and 3. the array period was reduced to 20 and 30 μm. By decreasing the angular step size, correlations over greater length scales are detected at the expense of increasing the data collection time. To compensate for this increase, the range of the angular measurements was also reduced. The net result was sensitivity to spatial correlations up to 70 μm. To effectively examine the long range correlations, it was still necessary to reduce the array period. For the experiments presented here, array periods of 20 and 30 μm were used.

Figures 2(a) and 2(b) show 20- and 30-μm period arrays, respectively, with cell nuclei visualized using fluorescence microscopy. The array sites were imaged using phase microscopy and superimposed on the fluorescence microscopy image of the nuclei. The arrays imaged in Figs. 2(a) and 2(b) show that although good registration was achieved at a number of sites, the array spacing was small enough to permit cells to bridge multiple sites. The effects of this registration are discussed later.
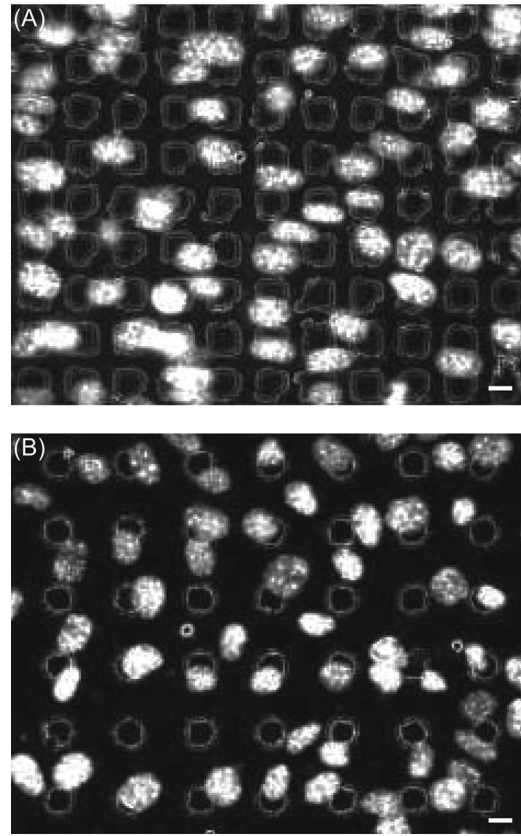

Fig. 2 Images of cell nuclei cultured on (a) 20-μm period microarray substrate and (b) 30-μm period microarray substrate. Cell nuclei are stained with Hoechst 33342 and imaged with fluorescence microscopy, and cell array sites are imaged using phase contrast microscopy and superimposed. Scale bars are 10 μm.

2.6 Theory

The light scattered by cells in the array can be analyzed using an elastic scattering formalism. In a previous theoretical examination[15] of the scattering of low coherence light by an ensemble of scatterers, Eq. (19) showed that the heterodyne signal at frequency δ due to wave vector component k for interferometrically detected scattered light can be written as:

$$I_b^k(\boldsymbol{q}_\perp, \Delta l) \propto \langle U_s^k U_r^{k*} + \text{cc} \rangle = \langle U_o^k U_o^{k*} \rangle \sum_n S_n(\boldsymbol{q}_\perp, k\hat{z})$$

$$\times \cos[k\Delta l + \delta t + \boldsymbol{r} \cdot (\boldsymbol{q}_\perp - k\hat{z})], \quad (2)$$

where U_o^k (U_s^k, U_r^k) is the incident (scattered, reference) field with wavevector k, the direction of which defines the z axis, and cc indicates the complex conjugate term. In this expression, the scattered field consists of a sum of the contribution from n scatterers, which has been mixed with a reference field with a variable direction of propagation, given by transverse wavevector $\boldsymbol{q}_\perp$ and variable path length Δl. The scattering amplitude S describes the change of momentum of incident light from the $\hat{z}$ direction to final direction $\boldsymbol{q}_\perp$.

The light scattered from a particular depth can be selectively detected by specifying the path length Δl of the reference field and integrating the selected signal across wavevec-

tor magnitudes. For a Gaussian distribution of frequencies centered at wavevector k_o, the demodulated mean square signal is given by:

$$\langle|I_b(\boldsymbol{q}_\perp)|^2\rangle_t \propto \sum_{n,m} S_n(\boldsymbol{q}_\perp, k_o\hat{z})S_m(\boldsymbol{q}_\perp, k_o\hat{z})\{\cos[\boldsymbol{r}_n \cdot (\boldsymbol{q}_\perp - k_o\hat{z})]$$

$$\times \cos[\boldsymbol{r}_m \cdot (\boldsymbol{q}_\perp - k_o\hat{z})]\}_t. \tag{3}$$

Here, the bandwidth of the source is assumed to be sufficiently broad to enable depth resolution, but narrow enough to allow the use of the center wavevector in the remaining terms describing the scattering process. If the contribution of the cells is assumed to be identical from cell to cell, the expression can be simplified as:

$$\langle|I_b(\boldsymbol{q}_\perp)|^2\rangle_t \propto |S(\boldsymbol{q}_\perp, k_o\hat{z})|^2 \sum_{n,m} \{\cos[(\boldsymbol{r}_n - \boldsymbol{r}_m) \cdot (\boldsymbol{q}_\perp - k_o\hat{z})]$$

$$+ \cos[(\boldsymbol{r}_n + \boldsymbol{r}_m) \cdot (\boldsymbol{q}_\perp - k_o\hat{z})]$$

$$= P(\boldsymbol{q}_\perp) \times T(\boldsymbol{q}_\perp), \tag{4}$$

where $P(\boldsymbol{q}_\perp) = |S(\boldsymbol{q}_\perp, k_o\hat{z})|^2$ is the form factor that describes the individual scattering process and $T(\boldsymbol{q}_\perp)$ is the structure factor that describes the spatial arrangement of the scatterers. For a periodic arrangement of scatterers, the difference $(\boldsymbol{r}_n - \boldsymbol{r}_m)$ and sum $(\boldsymbol{r}_n + \boldsymbol{r}_m)$ vectors are multiples of $\Delta\mathbf{r}$ such that $\boldsymbol{r}_n - \boldsymbol{r}_m$, $\boldsymbol{r}_n + \boldsymbol{r}_m = (n - m)\Delta\boldsymbol{r}$ and the expression for the structure factor can be written as:

$$T(\boldsymbol{q}_\perp) = \sum_w A_w\{\cos[w\Delta\boldsymbol{r} \cdot (\boldsymbol{q}_\perp - k_o\hat{z})]\}, \tag{5}$$

where A_w is a coefficient describing the occupation of the w various sites in the array. Examination of Eq. (5) shows that the structure factor will show periodic oscillations in $\boldsymbol{q}_\perp$ and associated higher harmonics, which are characteristic of the array spacing $\Delta\boldsymbol{r}$.

In a previous study,[2] it was shown that Fourier transformation of a/LCI measurements gives the correlation function of the density of the sample in the Born approximation. Similarly, Eq. (4) can be Fourier transformed to yield information about the spatial correlation of the cell samples:

$$\Im\langle|I_b(\boldsymbol{q}_\perp)|^2\rangle_t = \Im[P(\boldsymbol{q}_\perp) \times T(\boldsymbol{q}_\perp)] = \Gamma_P(r) * \Gamma_{LR}(r). \tag{6}$$

Here, the detected signal is Fourier transformed (FT) into the convolution of the individual cell correlation function (the FT of the form factor) and the long range correlation function (the FT of the structure factor). To isolate the long range correlations, the detected signal is divided by the form factor prior to Fourier transformation. This yields the correlation function describing intercellular order:

$$\Im\langle|I_b(\boldsymbol{q}_\perp)|^2/P(\boldsymbol{q}_\perp)\rangle_t = \Im[T(\boldsymbol{q}_\perp)] = \Gamma_{LR}(r). \tag{7}$$

The determination of the form factor from the detected signal is precisely the goal of our a/LCI analysis, thus it is straightforward to determine $\Gamma_{LR}(r)$ as a means to assess the long range correlations in the samples.
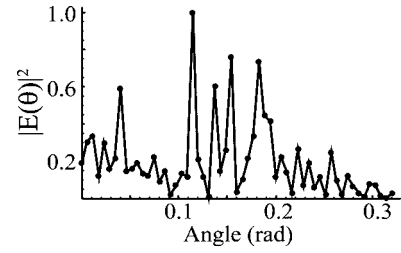

Fig. 3 Raw a/LCI data for light scattered by cells cultured on an array with 20-μm period. The data are the mean square heterodyne signal, given as a function of angle relative to the backscattering direction. Note the high frequency oscillations, characteristic of long-range order.

3 Results

3.1 Angle-Resolved Low Coherence Interferometry Data

Raw a/LCI data for light scattered by cells grown on a 20-μm period array are shown in Fig. 3, consisting of 57 points over an angular range of 0.32 rad. The striking feature in this data is the sharp oscillations in the angular distribution. The spatial correlations can be examined by taking the power spectrum for this data (Fig. 4). As shown previously,[2] the power spectrum of the angular distribution of the scattered field gives the two point spatial correlation of the sample in the Born approximation. The correlation data in Fig. 4 show correlations persisting over a 50-μm range.

To obtain nuclear size information, the data are low-pass filtered to suppress oscillations corresponding to correlations occurring over length scales greater than 20 μm. This cutoff was chosen to encompass the nucleus sizes observed in the micrographs. The data are then processed by removing the slowly varying background using a second-order polynomial, as described previously for a/LCI analysis.[2,6,10] The processed data are compared to similarly processed predictions of the Mie theory with the nuclear size determined by minimizing the chi-squared value between the data and Mie theory scattering distributions for ensembles of particles.[15] For the data shown in Fig. 3, the best fit was determined to be a Gaussian distribution of sizes with a 12.5±0.2-μm mean value, a 2.5% standard deviation (SD), and a refractive index of 1.043 relative to the cytoplasm. A comparison between the processed data and best-fit Mie theory is shown in Fig. 5. For experiments with 20- and 30-μm arrays, as well as cells grown on a substrate with no micropatterning as a control, a total of 27
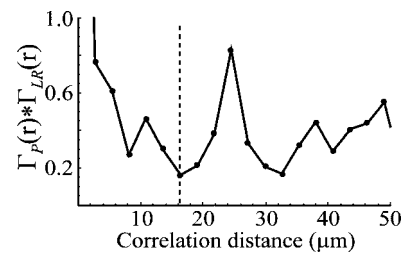

Fig. 4 Power spectrum of data shown in Fig. 3. The vertical line indicates the cutoff distance for the low-pass filter used in the a/LCI nuclear size analysis.
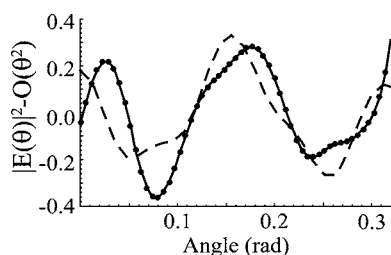
Fig. 5 Oscillatory component of scattering distribution (solid line), obtained via a/LCI analysis, shown compared to the best-fit oscillatory component of Mie theory scattering distribution (dashed line). The nuclear size obtained here is 12.4 μm.

samples were probed with a/LCI. The average nuclear diameter for these 27 samples was found to be 12.8±0.6 μm (Table 1) with an average SD of the size distribution of 2.5% of the mean diameter and an average refractive index of 1.043±0.008. The uncertainty in the mean diameter measurement is given by the 95% confidence interval for the average, defined by the standard deviation observed across the measurements, divided by the square root of the sample size multiplied by the appropriate t-distribution value (2.06). The a/LCI nuclear size data reported here differs slightly from previously presented results of this study.[16] The difference is due to the use of an improved analysis method, which allows for larger nucleus sizes (up to 20 μm), broader size distributions (up to 15% of the mean value), and a corrected center wavelength.

To examine the long range correlations, the detected signal is divided by the form factor, consisting of the obtained Mie solution and background distribution (not shown). The resulting distribution is then Fourier transformed to give the long range correlations [Fig. 6(a)], as shown in Eq. (7). Similarly processed long range correlations are shown for the 30-μm period array [Fig. 6(b)], and for the control sample consisting of cells cultured on an unpatterned substrate [Fig. 6(c)]. The data for the 20-μm period array, shown in Fig. 6(a), shows a sharp peak at a correlation distance of 24.5±2.7 μm with a full width at half maximum (FWHM) of 4.3 μm. The data for the 30-μm period array shows a sharp peak centered at a correlation distance of 31.0±2.8 μm [Fig. 6(b)], however, this peak is atop a broad pedestal with a FWHM of 27.6 μm. The data for the unpatterned control sample [Fig. 6(c)] show several peaks with comparable amplitudes and thus do not exhibit as clear of a correlation peak as seen with the patterned arrays. The distribution for the unpatterned arrays shown in Fig. 6(c) has a mean value of 30.4±2.8 μm with a FWHM of 22.2 μm. The average correlation distance seen for the 20-μm arrays was 24.5±3.0 μm (ten samples), while

Table 1 Nuclear diameter statistics from a/LCI and QIA data.

	Mean nuclear diameter (μm)	Standard deviation	Samples
a/LCI	12.8	1.7	27
QIA—total	13.1	1.9	172

Table 2 Nuclear spacing statistics from a/LCI and QIA data for both 20- and 30-μm period arrays. Correlation statistics for QIA are also presented from cells cultured without microarray substrates.

	Mean nuclear spacing (μm)	Standard deviation	Samples
a/LCI 20-μm array	24.5	4.8	10
QIA 20-μm array	24.0	3.5	38
a/LCI 30-μm array	31.9	5.3	6
QIA 30-μm array	30.1	5.6	61
QIA no array	35.0	11.7	44

that seen for the 30-μm array was 31.9±4.3 μm (six samples). These results are summarized in Table 2. As a final note, the long range correlation data presented here also differ from the initial presentation of this study,[16] as a new, more rigorous analysis method has been used based on the theory presented earlier.

3.2 Image Analysis

The diameter for 172 nuclei was determined using QIA, and the resulting distribution was found to form a Gaussian distribution of sizes with a mean of 13.1 μm and a SD of 1.9 μm, resulting in a 95% confidence interval of 12.8 to 13.4 μm. These results are compared to the a/LCI results in the discussion in Sec. 4. In addition to using QIA to analyze the nuclear diameter, the long range correlations were examined by calculating the autocorrelation function for fluorescence microscopy images of cells in the 20 μm, 30 μm, and unpatterned arrays. The average spacing for the 20-μm period arrays was found to be 24.0±1.1 μm, which included data for 38 cell pairs. The average spacing for the 30-μm period arrays was found to be 30.1±1.4 μm, which included data for 61 cell pairs (Table 2). Representative data are presented for the 20 - and 30-μm arrays in Figs. 7(a) and 7(b) with the nearest-neighbor spacing determined to be 23.7 and 29.3 μm, respectively. The correlations are seen to extend for multiple neighbor spacings, with the second neighbor spacing being measured at 48.4 and 58.5 μm, respectively, or roughly double the first neighbor spacing for the 20- and 30-μm arrays. For cells cultured without an underlying microarray pattern, the average nearest-neighbor distance determined by QIA was found to be 35.0±3.5 μm. Comparison to the a/LCI long range correlation data is presented next.

4 Discussion

The a/LCI data obtained for the NIH/3T3 cells grown on micropatterned and unpatterned substrates have been analyzed to determine the size of the cell nuclei and the long range correlations in the sample. On comparison with the QIA results of nuclear size, which yielded an average size of 13.1 μm, the a/LCI data yield a slightly smaller average size (12.8 μm), but within the calculated 95% confidence interval. Thus, the low-pass filtering step in the a/LCI analysis routine can remove the effects of high frequency oscillations due to long range correlations, and permit accurate determination of
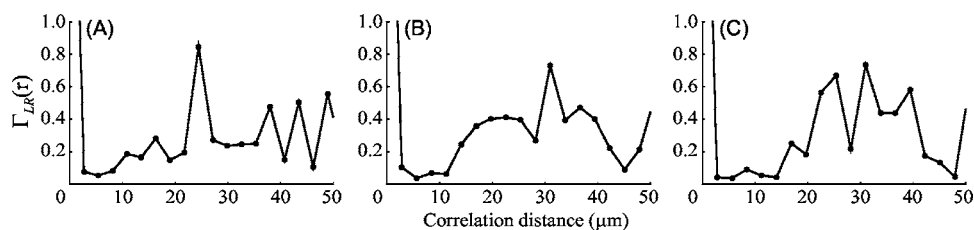
Fig. 6 Long range correlations for the *in-vitro* samples. (a) 20-μm period array with a narrow correlation peak at 24.1 μm, (b) 30-μm period array with a narrow correlation peak at 31.0 μm, and (c) control sample without micropatterned array showing a broad distribution with a peak at 30.4 μm.

the size of the cell nuclei, regardless of long range order imposed by the use of a micropatterned substrate.

The correlation data in Fig. 6 demonstrate that the a/LCI system detects correlations over length scales that are large compared to the nuclear size. To assess the accuracy of these measurements, the a/LCI results were compared to autocorrelation data obtained via QIA. The average spacing for the 20-μm period arrays was found to be 24.0$\pm$1.1 μm with QIA (38 cell pairs) and 24.5$\pm$3.0 μm (ten samples) for the a/LCI measurements. The average spacing for the 30-μm period arrays was found to be 30.1$\pm$1.4 μm (61 cell pairs) with QIA, and 31.9$\pm$4.3 μm (six samples) for the a/LCI measurements. Thus, good agreement is obtained between the a/LCI long range correlation data and the QIA data with the larger uncertainty in the average a/LCI data due to the smaller sample size.

In the long range correlation data, there is a significant difference between the measured average nuclei spacing (both a/LCI and QIA) and the 20-μm period of the array. This difference can be understood by considering that cells on neighboring sites were overcrowded, forcing some cells to bridge two array sites and preventing cells from occupying every array site. Because all cells were not centered on array

Fig. 7 1-D spatial autocorrelation function of nuclear fluorescence microscopy images (Fig. 2) on (a) 20-μm period substrate and (b) 30-μm period substrate. The nonzero correlation peaks are 23.7 and 48.4 μm for the 20-μm period array and 29.3 and 58.5 μm for the 30-μm period array. The first peak is the nearest-neighbor spacing and the second peak is the second neighbor spacing. Note the good agreement to the correlation distances in Fig. 6 as determined by a/LCI.

sites, the distance between nuclei was slightly increased over the predicted value of 20 μm. This phenomenon is not as prevalent with the 30-μm array samples due to the array spacing being closer to the natural center-to-center cell spacing.

Another significant difference between the QIA and a/LCI data is the widths of the observed correlations peaks. The QIA autocorrelation data consistently yield peaks with widths of approximately the nucleus diameter (Fig. 7), while the a/LCI data exhibit correlation peaks with narrow widths and features with broad widths (Fig. 6). This effect is due to the differences in the way the correlation data is calculated. The QIA data is determined by observing the spacing between nearest-neighbor nuclei over the range of the micrograph, which is a convolution of the nuclear size and the long range correlations. In comparison, the a/LCI data has been processed to yield just the long range correlation information using the theory outlined earlier. To obtain similar information from the QIA data, a deconvolution process can be applied. This would simply narrow the observed correlation peaks without changing their mean value. Thus, the comparison of the mean correlation distances would not be affected by this additional processing step.

For cells grown on unpatterned substrates, the a/LCI long range correlation data [Fig. 6(c)] show several peaks that are comparable in amplitude to the peaks seen in the data for the 20- and 30-μm period arrays. In addition, the data for the cells on unpatterned substrates do not demonstrate a correlation distance that can be clearly identified as a peak correlation. However, the broad distribution seen in the data for unpatterned arrays can be modeled as a Gaussian distribution with a mean value of 30.4 mm and a SD of 13.0 μm. The QIA of these samples yields a mean correlation distance of 35.0 μm with a large SD of 11.7 μm. This large SD is exemplified in the broad distribution of long range correlation distances seen in Fig. 6(c). Furthermore, the peak value of Fig. 6(c) is well within the expected range. The mean internuclear distance value of 35.0 μm is a reasonable approximation of the average size of NIH/3T3 cells, and the SD indicates a significantly broader distribution of internucleus distances than that observed with the patterned arrays. This finding is consistent with the unordered random nature of the growth patterns of NIH/3T3 fibroblast cells. This is in contrast to the symmetric spacing imposed on the fibroblasts by the arrays, or in other cell systems such as epithelial cells, which tend to grow in a regular pattern on a large scale.
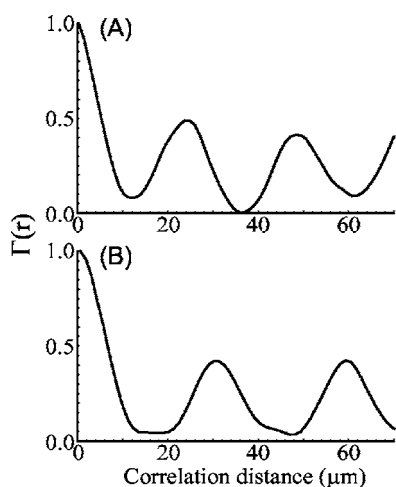
5   Summary

In summary, we use a/LCI to examine angle-resolved scattering from NIH/3T3 cells grown on micropatterned substrates. The primary goal of this study is to assess the role of long range correlations on a/LCI analysis. It is found that long range correlations are accurately identified by a/LCI, and their effects are suppressed effectively using a low-pass filter to yield accurate nuclear size data. Future work in this area will examine the utility of long range correlations to detect changes in tissue architecture associated with neoplastic transformation, which may increase the already high accuracy of a/LCI in identifying and differentiating stages of precancerous tissue growth.

References

1. V. Backman, V. Gopal, M. Kalashnikov, K. Badizadegan, R. Gurjar, A. Wax, I. Georgakoudi, M. Mueller, C. W. Boone, R. R. Dasari, and M. S. Feld, "Measuring cellular structure at submicrometer scale with light scattering spectroscopy," *IEEE J. Sel. Top. Quantum Electron.* **7**(6), 887–893 (2001).
2. A. Wax, C. H. Yang, V. Backman, K. Badizadegan, C. W. Boone, R. R. Dasari, and M. S. Feld, "Cellular organization and substructure measured using angle-resolved low-coherence interferometry," *Biophys. J.* **82**(4), 2256–2264 (2002).
3. J. R. Mourant, T. M. Johnson, S. Carpenter, A. Guerra, T. Aida, and J. P. Freyer, "Polarized angular dependent spectroscopy of epithelial cells and epithelial cell nuclei to determine the size scale of scattering structures," *J. Biomed. Opt.* **7**(3), 378–387 (2002).
4. J. D. Wilson, C. E. Bigelow, D. J. Calkins, T. H. Foster, "Light scattering from intact cells reports oxidative-stress-induced mitochondrial swelling," *Biophys. J.* **88**(4), 2929–2938 (2005).
5. V. Backman, M. B. Wallace, L. T. Perelman, J. T. Arendt, R. Gurjar, M. G. Muller, Q. Zhang, G. Zonios, E. Kline, T. McGillican, S. Shapshay, T. Valdez, K. Badizadegan, J. M. Crawford, M. Fitzmaurice, S. Kabani, H. S. Levin, M. Seiler, R. R. Dasari, I. Itzkan, J. Van Dam, and M. S. Feld, "Detection of preinvasive cancer cells," *Nature (London)* **406**(6791), 35–36 (2000).
6. A. Wax, C. H. Yang, M. G. Muller, R. Nines, C. W. Boone, V. E. Steele, G. D. Stoner, R. R. Dasari, and M. S. Feld, "*In situ* detection of neoplastic transformation and chemopreventive effects in rat esophagus epithelium using angle-resolved low-coherence interferometry," *Cancer Res.* **63**(13), 3556–3559 (2003).
7. R. Drezek, M. Guillaud, T. Collier, I. Boiko, A. Malpica, C. Macaulay, M. Follen, and R. Richards-Kortum, "Light scattering from cervical cells throughout neoplastic progression: influence of nuclear morphology, DNA content, and chromatin texture," *J. Biomed. Opt.* **8**(1), 7–16 (2003).
8. L. B. Lovat, D. Pickard, M. Novelli, P. M. Ripley, H. Francis, I. J. Bigio, and S. G. Bown "A novel optical biopsy technique using elastic scattering spectroscopy for dysplasia and cancer in Barrett's esophagus," *Gastrointest Endosc* **51**(4), Ab227–Ab227 (2000).
9. A. Wax, C. H. Yang, R. R. Dasari, and M. S. Feld, "Measurement of angular distributions by use of low-coherence interferometry for light-scattering spectroscopy," *Opt. Lett.* **26**(6), 322–324 (2001).
10. J. W. Pyhtila, R. N. Graf, and A. Wax, "Determining nuclear morphology using an improved angle-resolved low coherence interferometry system," *Opt. Express* **11**(25), 3473–3484 (2003).
11. A. Wax, C. Yang, V. Backman, M. Kalashnikov, R. R. Dasari, and M. S. Feld "Determination of particle size using the angular distribution of backscattered light as measured with low-coherence interferometry," *J. Opt. Soc. Am. A* **19**, 737–744 (2002).
12. A. Wax J. W. Pyhtila, R. N. Graf, R. Nines, C. W. Boone, R. R. Dasari, M. S. Feld, V. E. Steele, and G. D. Stoner, "Prospective grading of neoplastic change in rat esophagus epithelium using angle-resolved low coherence interferometry," *J. Biomed. Opt.* **10**, 051604 (2005).
13. J. H. Hyun, H. W. Ma, Z. P. Zhang, T. P. Beebe, and A. Chilkoti, "Universal route to cell micropatterning using an amphiphilic comb polymer," *Adv. Mater. (Weinheim, Ger.)* **15**(7-8), 576–579 (2003).
14. H. W. Ma, J. H. Hyun, Z. Zhang, T. P. Beebe, Jr., and A. Chilkoti, "Fabrication of biofunctionalized quasi-three-dimensional microstructures of a nonfouling comb polymer using soft lithography," *Adv. Funct. Mater.* **15**(4), 529–540 (2005).
15. A. Wax, "Low-coherence light-scattering calculations for polydisperse size distributions," *J. Opt. Soc. Am. A* **22**(2), 256–261 (2005).
16. J. W. Pyhtila and A. Wax, "Coherent light scattering by in vitro cell arrays observed with angle-resolved low coherence interferometry," *Proc. SPIE* **5690**, 334–341 (2005).